Electronic structure of $FePO_4$, $LiFePO_4$, and related materials

Ping Tang and N. A. W. Holzwarth*
Department of Physics, Wake Forest University, Winston-Salem, North Carolina 27109, USA
(Received 21 June 2003; revised manuscript received 25 August 2003; published 29 October 2003)

The electronic structures of $FePO_4$ and $LiMPO_4$, where $M=$Mn, Fe, Co, and Ni, are studied within the framework of density-functional theory. These materials have interesting magnetic properties and have promising technological interest as cathode materials in rechargeable batteries. A comparison of results for various spin configurations suggests that the ferromagnetic configuration, while not seen experimentally, can serve as a useful approximation for studying general features of the electronic structure. The partial densities of states and contour plots of electron densities show that covalent bonding between Fe $3d$ and O $2p$ orbitals is greater in $FePO_4$ than in $LiFePO_4$. Nevertheless, $LiFePO_4$ is calculated to have a greater binding energy than its $FePO_4$ and Li metal components; the corresponding open circuit voltage for the cathode discharge is calculated to be 3.2 V, which is comparable to (although smaller than) the experimentally measured value.

DOI: 10.1103/PhysRevB.68.165107 PACS number(s): 71.20.Ps, 71.15.Mb, 71.15.Nc, 75.50.Bb

I. INTRODUCTION

Crystals of $LiFePO_4$ and related materials have recently received a lot of attention due to their very promising use as cathodes in rechargeable lithium ion batteries. A paper by Padhi, Nanjundaswamy, and Goodenough[1] in 1997 introduced $LiFePO_4$ as a viable alternative to some of the transition metal oxides that are currently used in commercial batteries. Current cathode materials—$LiCoO_2$, $LiNiO_2$, and $LiMn_2O_4$—suffer from deterioration with use or at moderately higher temperatures and also have raised environmental concerns with their disposal.[1–3] By contrast, $LiFePO_4$ is much more stable, while having similar theoretical capacity and voltage characteristics as well as possible cost and environmental advantages.[1,4,5] There has been extensive developmental work focused on increasing the electrical conductivities of $LiFePO_4$ and $FePO_4$, in order to optimize their cathodic performance as summarized in several recent review papers.[6–8]

Coincidentally, low temperature studies of the $LiMPO_4$ compounds, where $M=$Mn, Fe, Co, and Ni, have revealed that the materials also have very interesting magnetic behaviors with antiferromagnetic ground states.[9–11] Recent studies of the magnetic susceptibility as a function of temperature[12] show that the room-temperature behavior follows a Curie-Weiss model with well-defined magnetic moments associated with the transition metal sites and a negative Curie temperature consistent with the behavior of an antiferromagnetic material at temperatures above its Néel point. While the magnetic properties of these materials may not have direct technological use, they do affect the electronic states of the materials which determine their electrochemical behavior.

In order to take the first step toward developing realistic simulations of structural, electronic, and magnetic properties of these materials, we have performed a series of electronic structure calculations within the framework of density-functional theory.[13,14] While simulation work on the $LiFePO_4$ family of materials is relatively new,[15–17] we note that computer simulations on other electrode materials[18–22] have been very successful for advancing both basic materials physics and technological development.

The calculational method is briefly discussed in Sec. II. The crystal structures are described in Sec. III. Section IV A presents results for various spin configurations. Section IV B analyzes the calculated total energies. Section IV C presents the spectral results for the one-electron states. The summary and conclusions are given in Sec. V.

II. CALCULATIONAL METHODS

Self-consistent electronic structure calculations were performed within the framework of density-functional theory[13,14] using the WIEN2K code[23] which is based on the linearized augmented plane-wave method (LAPW) of Andersen.[24]

The calculational parameters used in this work are as follows. The muffin-tin radii (R_{MT}) were 2.0 bohrs for Li and M, and 1.38 bohrs for P and O. These radii were also used for determining the weighting of the partial densities of states for each atomic type and for integrating the net electron spin within each muffin-tin sphere. The wave functions were represented using the so-called "APW+lo" basis[25] inside the muffin-tin spheres and plane waves with wave vectors $\leqslant 5.1$ bohrs^{-1} in the interstitial region, where "lo" represents local orbitals. The integrals over the Brillouin zone were done using a tetrahedron method[26] with a **k**-point sampling based on a uniform grid with $3\times5\times6$ divisions in the **a**, **b**, and **c** directions, respectively. For $LiMnPO_4$, $LiCoPO_4$, and $LiNiPO_4$ a smaller grid ($2\times5\times6$) was used. We verified that these choices for the computational parameters ensured that total energy differences were converged to better than 0.01 eV.

For most of the calculations, the exchange-correlation functional was the local spin-density approximation ("LSDA") form of Perdew and Wang,[27] while a few of the calculations used the generalized gradient ("GGA") form of Perdew, Burke, and Ernzerhof.[28] It is well known that there are limitations in these functionals, particularly in predicting the band gaps[29] and in including unphysical electron self-interactions[30] which can be significant for transition-metal materials. However, this study provides a well-defined basis for more sophisticated treatments in the future.

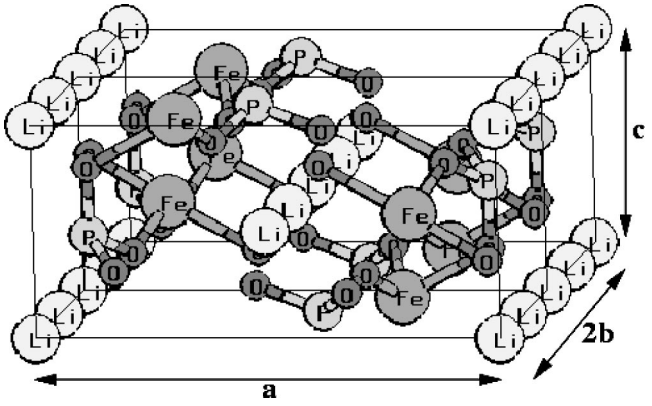

FIG. 1. Crystal structure of $LiFePO_4$ showing two unit cells constructed using XCrySDen (Ref. 33).

For some of the materials, we optimized the structural and lattice parameters. For a given set of lattice parameters, the WIEN2K code moves the independent atoms into their equilibrium positions on the basis of the calculated forces. We performed these optimizations for a grid of lattice constants and found the optimal lattice constants using a polynomial interpolation. Although the results were surprisingly sensitive to the **k**-point sampling, reasonable accuracy could be obtained by performing each optimization calculation using a $(1\times2\times2)$ sampling grid, which reduces to a single **k** point because of crystal symmetry. The total energies of the optimized structures were then determined using the $(3\times5\times6)$ **k**-point sampling grid discussed above, checking that the forces on the atoms remained small.

III. CRYSTAL STRUCTURES

The materials in this study form the olivine structure[31] with the symmetry group *Pnma*, which is listed as no. 62 in the *International Tables for Crystallography*.[32] Figure 1 shows a ball and stick diagram of the $LiFePO_4$ crystal structure. The O sites form a nearly tetrahedral arrangement about each P site and also form an approximately octahedral arrangement about each Fe site. From the diagram, it is apparent that there are channels along the *b* axis which accommodate the mobile Li^+ ions. When Li^+ ions and electrons are removed from $LiFePO_4$, the remaining $FePO_4$ framework has same structure, with a small (7%) reduction in volume.

The fact that most of these materials are naturally occurring minerals[34] is encouraging evidence of their structural stability. $LiFePO_4$ is known as ''triphylite.'' It has the same structure as $LiMnPO_4$ which is known as ''lithiophilite'' and the two form a complete solid-solution series. The delithiated forms of the materials $FePO_4$ and $MnPO_4$ are known as ''heterosite'' and ''purpurite,'' respectively. While the *Pnma* structure of $FePO_4$ formed from delithiating $LiFePO_4$ is well established, there does not appear to be experimental evidence that other MPO_4 materials have stable *Pnma* structures. In particular, the Cambridge Structural Database[35] does not list *Pnma* structures for $MnPO_4$, $CoPO_4$, or $NiPO_4$. In fact $FePO_4$ is also known to have a quartz-like form.[36] Synthetic crystals of $LiMPO_4$ have been prepared by heating stoichiometric amounts of the constituents in an inert atmosphere.[1,37–40] A new promising synthesis technique based on ''carbothermal reduction'' has recently been reported by Barker and co-workers.[40]

TABLE I. Experimental lattice constants for stoichiometric materials in the *Pnma* (62) structure.

	Ref.	a(Å)	b(Å)	c(Å)	V (Å)^3
$LiMnPO_4$	38	10.431	6.0947	4.7366	301.12
$LiFePO_4$	38	10.227	6.0048	4.6918	288.12
	1	10.334	6.008	4.693	291.392
	41	10.332	6.010	4.692	291.4
	42	10.3290	6.0065	4.6908	291.02
	40	10.288	5.976	4.672	287.23
$LiCoPO_4$	43	10.2001	5.9199	4.690	283.2
$LiNiPO_4$	38	10.0275	5.8537	4.6763	274.49
$FePO_4$	42	9.8142	5.7893	4.7820	271.7
	1	9.821	5.792	4.788	272.357

Table I summarizes *Pnma* structural parameters which have appeared in the literature. Each unit cell contains four formula units of the compound. The first entry in the table for each material represents the lattice constants used in the present work. The internal parameters for the *M*, P, and O sites were taken from those references. Some of these will be discussed further in Sec. IV B.

IV. RESULTS

A. Spin configurations

The calculations were performed using three different spin configurations. Their abbreviations are explained below.

(1) NS (no spin): These results were obtained by forcing double occupancy of each band.

(2) FM (ferromagnetic): These results were obtained by allowing unrestricted spin polarization within the unit cell.

(3)AF (antiferromagnetic): These results were obtained by forcing opposite spins on sites related by inversion symmetry within the unit cell, as is consistent with experimental antiferromagnetic structure at low temperature.[9–11]

Since spin-orbit interactions were not included in the calculations, the spin orientations are not related to the crystallographic directions. The $\uparrow$ spin direction is arbitrarily identified with the majority spin for the FM calculations, while the $\uparrow$ and $\downarrow$ states are equivalent in the AF calculations.

Table II shows the differences in the total energy of each material in the nonspin polarized configuration relative to its total energy in the ferromagnetic configuration. From these results, we see that for all of the materials, the ferromagnetic spin configurations are much more stable than the nonspin polarized configurations. For $FePO_4$, the FM spin stabilization is more than 1 eV and for $LiFePO_4$ it is $\approx$1.5 eV. For both materials, the spin stabilization energies are larger for the GGA exchange-correlation form than for the LSDA form. For the $LiMPO_4$ series of materials, the FM spin stabilization energy monotonically increases with the number of un-

TABLE II. Calculated total energy differences $E_{\text{total}}(\text{NS}) - E_{\text{total}}(\text{FM})$ and $E_{\text{total}}(\text{AF}) - E_{\text{total}}(\text{FM})$, given in units of eV/formula unit. The calculations were done using the LSDA (Ref. 27) and GGA (Ref. 28) exchange-correlation functionals as noted.

		NS	AF
$FePO_4$	(LSDA)	1.10	−0.15
	(GGA)	1.31	−0.14
$LiFePO_4$	(LSDA)	1.45	0.02
	(GGA)	1.61	−0.03
$LiMnPO_4$	(LSDA)	2.69	0.12
$LiCoPO_4$	(LSDA)	0.79	
$LiNiPO_4$	(LSDA)	0.47	0.11

paired electrons in the $3d$ shell of the transition metal M. The smallest is for $M=\text{Ni}$ (d^8) and the largest energy is for $M=\text{Mn}$ (d^5).

Table II also shows the differences in the total energy of each material in the antiferromagnetic configuration relative to its total energy in the ferromagnetic configuration. These energy differences are very small—of the order of 0.1 eV or less for all of the materials. The energy difference for $LiFePO_4$ is the smallest of the materials studied. Since low-temperature antiferromagnetic phases have been found experimentally[9–11,44,45] for $LiMPO_4$ ($M=$Mn, Fe, Co, and Ni), we would expect the energies in the AF column of Table II to be negative. The extent to which this is not true provides a measure of the inaccuracies in the calculational model. More accurate calculations should include correlation energy corrections beyond LSDA and GGA, and also include spin-orbit interactions in order to describe the coupling of the spins to the lattice. These more accurate calculations may reveal spin configurations in addition to those considered here. On the other hand, the fact that the energy difference between the FM and AF configurations are calculated to be small, and that much of the interest in these materials is focused on their room-temperature behavior which has no spin ordering, provides a justification for focusing on the FM configuration for approximately representing these materials within the present formalism.

Room-temperature measurements of the magnetic susceptibility of these materials[12,46] follow a Curie-Weiss model from which it is possible to extract an effective local magnetic moment associated with the M sites. The spin-polarization density calculated for the ferromagnetic and antiferromagnetic configurations should be related to the measured moments. The calculations give several possible measures of spin. For example, the spin polarization integrated within the muffin-tin sphere of the M sites can be determined according to

$$\sigma_{\text{Sphere}} \equiv \int_{|\mathbf{r}-\mathbf{R}_M| \le R_{MT}} d^3r [n^{\uparrow}(\mathbf{r}) - n^{\downarrow}(\mathbf{r})] \tag{1}$$

for either the ferromagnetic or antiferromagnetic spin configuration. These values are listed in Table III, showing that the GGA results favor slightly higher spin polarization relative to the LSDA results and that spin polarization within the muffin-tin sphere is slightly larger in the ferromagnetic configuration than in the antiferromagnetic configuration. Also the number of unpaired spins in the ferromagnetic configuration averaged over a unit cell and divided by the number of formula units per cell, $\sigma^{FM}_{\text{Unit}}$, is shown in Table III. (The corresponding quantity for the antiferromagnetic configuration is identically 0.) These take simple integer values which exactly follow Hund's rules for the transition metal ions. Since for all of these materials the transition metal d-electron densities extend beyond the muffin-tin radius, it is not surprising that $\sigma_{\text{Sphere}} < \sigma^{FM}_{\text{Unit}}$. If it is assumed that the number of unpaired spins per formula unit is associated with the z component of the total spin quantum number for the M site,

$$S_z = \frac{\hbar}{2} \sigma^{FM}_{\text{Unit}}, \tag{2}$$

TABLE III. Calculated spin polarizations within muffin-tin spheres $\sigma^{FM}_{\text{Sphere}}$ and $\sigma^{AF}_{\text{Sphere}}$ [Eq. (1)] for the ferromagnetic and antiferromagnetic configurations, respectively. In addition, the number of unpaired spins per formula unit in the ferromagnetic configuration (denoted $\sigma^{FM}_{\text{Unit}}$) are used to estimate local magnetic moments according to Eq. (3) and compared with the experimental moments in units of μ_B.

		$\sigma^{FM}_{\text{Sphere}}$	$\sigma^{AF}_{\text{Sphere}}$	$\sigma^{FM}_{\text{Unit}}$	$\mu^{\text{est.}}_{\text{eff}}$	$\mu^{\text{exp.}}_{\text{eff}}$
$FePO_4$	(LSDA)	3.95	3.83	5	5.9	
	(GGA)	4.00	3.91	5		
$LiFePO_4$	(LSDA)	3.46	3.40	4	4.9	5.45 (Ref. 11)
	(GGA)	3.49	3.45	4		5.41 (Refs. 46 and 47)
						6.8 (Ref. 12)
$LiMnPO_4$	(LSDA)	4.30	4.27	5	5.9	5.95 (Ref. 11)
						5.4 (Ref. 12)
$LiCoPO_4$	(LSDA)	2.54	2.45	3	3.9	5.7 (Ref. 45)
						4.85 (Refs. 46 and 47)
						5.16 (Refs. 9 and 47)
						5.1 (Ref. 12)
$LiNiPO_4$	(LSDA)	1.58	1.44	2	3.2	3.35 (Ref. 45)
						3.1 (Ref. 12)

and if we approximate the electron g factor with its free-electron value, we can estimate the local magnetic moments according to

$$\mu_{\rm eff}^{\rm est.} = \mu_B \frac{g}{2} \sqrt{\sigma_{\rm Unit}^{FM}(\sigma_{\rm Unit}^{FM}+2)}. \quad (3)$$

In Table III we compare these values with the experimental values of the effective local moments obtained by fitting the temperature dependence of the magnetic susceptibility to a Curie-Weiss form. While the experimental measurements vary with each other, in general the results indicate that $\mu_{\rm eff}^{\rm est.} < \mu_{\rm eff}^{\rm exp.}$, suggesting that a more sophisticated analysis is needed.

B. Structural optimization and total energy results for Li_xFePO_4

The total energy results can be used to analyze the cathode reaction and voltage. The discharge reaction for the cathode should have the form

$$FePO_4 + x\,Li^+ + x\,e^- \rightarrow Li_xFePO_4, \quad (4)$$

where Li_xFePO_4 represents a nonstoichiometric form of the material. The open circuit voltage for this process relative to a Li metal anode can be approximated from a total energy difference expression if entropy and volumetric effects can be ignored:[18]

$$e\Delta V_1 \approx \frac{E_{\rm total}(FePO_4) + xE_{\rm total}(Li) - E_{\rm total}(Li_xFePO_4)}{x}, \quad (5)$$

where $E_{\rm total}$ denotes the total energy relative to a single formula unit.

However, Padhi and co-workers[1] presented evidence that the nonstoichiometric compound Li_xFePO_4 is unstable relative to a two-phase form containing $FePO_4$ and $LiFePO_4$ crystallites, so that the reaction is instead given by

$$FePO_4 + x\,Li^+ + x\,e^- \rightarrow x\,LiFePO_4 + (1-x)FePO_4. \quad (6)$$

In this case, the open circuit voltage would be

$$e\Delta V_2 \approx E_{\rm total}(FePO_4) + E_{\rm total}(Li) - E_{\rm total}(LiFePO_4), \quad (7)$$

which is independent of x.

However, in order for the cathode reaction to occur, nonstoichiometric material Li_xFePO_4 must exist for some period of time, perhaps in a meta-stable state. In order to assess the stability of the nonstoichiometric material, we need to examine the total energies difference:

$$\Delta E_{12}(x) \equiv E_{\rm total}(Li_xFePO_4) - [xE_{\rm total}(LiFePO_4) + (1-x)E_{\rm total}(FePO_4)]. \quad (8)$$

In order to properly calculate the voltages (5) and (7) and the stability of the partially charged materials (8), it is necessary to work with the theoretical ground states of the systems, which often differ slightly from the experimental structures. We restricted our attention to the LSDA form of the exchange-correlation functionals and to the ferromagnetic spin configurations for optimizing the structures of $FePO_4$, $LiFePO_4$, and a representative partially charged structure. The nonstoichiometric structure constructed for this evaluation (A) has $x=\frac{1}{2}$ and is formed from the experimental structure of $LiFePO_4$,[38] by removing every other Li^+ ion along the b axis and assuming $P2_1/a$ symmetry. We also briefly considered another structure (B), formed by removing one b-axis channel of Li^+ ions per unit cell, and assuming $P2_1/m$ symmetry. These symmetries are listed[32] as structures 14 and 11, respectively.

TABLE IV. Optimized lattice parameters for Li_xFePO_4 materials. The relaxation energies $\Delta E_{\rm relax}$ (total energy difference of optimized structure relative to structure taken from experiment) is given in the last column in units of eV/formula unit.

	a(Å)	b(Å)	c(Å)	V(Å)^3	$\Delta E_{\rm relax}$
$LiFePO_4$	10.06	5.89	4.64	274.8	−0.21
$Li_{1/2}FePO_4(A)$	9.96	5.83	4.70	273.1	−0.44
$FePO_4$	9.81	5.79	4.78	271.7	−0.07

Table IV lists the values of the optimized lattice parameters and the relaxation energies and Table V lists the optimized internal parameters compared with the experimental values obtained in this study. The ''experimental'' structures for $LiFePO_4$ and $FePO_4$ were taken from Refs. 38 and 42, respectively. While the lattice parameters for $FePO_4$ are identical to the experimentally measured values, the internal parameters changed slightly to yield a small relaxation energy. For $LiFePO_4$, the lattice constants are calculated to be approximately 2% smaller than their experimental values and the relaxation energy is much greater. The nonstoichiometric

TABLE V. Experimental and optimized positions of unique atoms for Li_xFePO_4 materials, given in terms of fractional coordinates (x,y,z) corresponding to $x\mathbf{a}+y\mathbf{b}+z\mathbf{c}$.

		Experimental	Optimized
$LiFePO_4$:	Li	(0.00, 0.00, 0.00)	(0.00, 0.00, 0.00)
	Fe	(0.29, 1/4, 0.97)	(0.28, 1/4, 0.98)
	P	(0.09, 1/4, 0.43)	(0.09, 1/4, 0.42)
	O_1	(0.09, 1/4, 0.75)	(0.09, 1/4, 0.75)
	O_2	(0.45, 1/4, 0.19)	(0.45, 1/4, 0.21)
	O_3	(0.17, 0.05, 0.30)	(0.17, 0.04, 0.29)
$Li_{1/2}FePO_4(A)$:	Li		(0.00, 0.00, 0.00)
	Fe		(0.28, 0.26, 0.98)
	P		(0.10, 0.24, 0.42)
	O_1		(0.11, 0.23, 0.75)
	O_2		(0.45, 0.24, 0.18)
	O_3		(0.17, 0.04, 0.27)
	O_4		(0.32, 0.55, 0.80)
$FePO_4$:	Fe	(0.28, 1/4, 0.95)	(0.27, 1/4, 0.95)
	P	(0.09, 1/4, 0.39)	(0.09, 1/4, 0.40)
	O_1	(0.12, 1/4, 0.71)	(0.12, 1/4, 0.71)
	O_2	(0.44, 1/4, 0.17)	(0.44, 1/4, 0.15)
	O_3	(0.17, 0.05, 0.25)	(0.17, 0.04, 0.25)

TABLE VI. Experimental and optimized nearest-neighbor distances (in Å) for Li_xFePO_4.

		Experimental	Optimized
$LiFePO_4$:	P—O	1.50,1.53,1.53,1.57	1.53,1.54,1.56,1.56
	Fe—O	1.98,2.04,2.04,2.23, 2.29, 2.29	2.02,2.02,2.05,2.13, 2.17,2.17
	Li—O	2.14,2.14,2.15,2.15, 2.24,2.24	2.05,2.05,2.10,2.10, 2.16,2.16
$Li_{1/2}FePO_4(A)$:	P—O		1.52,1.53,1.56,1.57
	Fe—O		1.98,1.99,2.00,2.06, 2.11,2.16
	Li—O		2.10,2.10,2.10,2.10, 2.13,2.13
$FePO_4$:	P—O	1.54,1.54,1.55,1.55	1.52,1.52,1.56,1.56
	Fe—O	1.88,1.94,2.04,2.04, 2.14,2.14	1.88,1.90,2.04,2.04, 2.14,2.14

structure *A* is found to have lattice parameters between those of $FePO_4$ and $LiFePO_4$ and has a substantial relaxation energy relative to its assumed structure. The optimized internal coordinates listed in Table V are very close to the corresponding experimental values. Perhaps an easier way of quantifying the structural differences is in terms of the nearest-neighbor distances. These are listed in Table VI. Although the differences between the experimental and optimized structures are of the same order of magnitude as differences between various experimental results,[38,41] it is possible to make some general comments. In general, we find that the optimized structures are calculated to have generally smaller bond lengths than the experimental values, with the exception of the P—O bonds in $LiFePO_4$. This trend is consistent with the known trend of LSDA calculations to overestimate the binding of most materials. For both the experimental and the optimized structures, the average nearest-neighbor Fe—O bond lengths increase with increasing Li content.

Having calculated the optimized structures for these materials and their corresponding total energies, we are now in a position to determine the open circuit voltages and the stability energies [Eqs. (5), (7), and (8)]. This is shown in Table VII, where we compare the results calculated using the experimental and optimized structures. For simulating the electronic structure of lithium metal, the bcc lattice constant of $a=3.491$ Å was used[48] for the ''experimental'' structure.

TABLE VII. Calculated open circuit voltages and stability energies (per formula unit) for Li_xFePO_4 calculated using Eqs. (5), (7), and (8), comparing results in experimental and optimized structures.

	Experimental	Optimized
ΔV_2	3.07 V	3.20 V
$\Delta V_1(x=\frac{1}{2})(A)$	2.97 V	3.71 V
$\Delta V_1(x=\frac{1}{2})(B)$	2.50 V	
$\Delta E_{12}(x=\frac{1}{2})(A)$	0.05 eV	−0.25 eV
$\Delta E_{12}(x=\frac{1}{2})(B)$	0.28 eV	

The optimized structure reduced the total energy by 0.01 eV.

The results for the open circuit voltages listed in Table VII show that the calculated voltage increases when structural relaxation is taken into account. The value of ΔV_2 calculated for the optimized structure is not too far from the experimental value of 3.5 eV.[1] The calculated voltages $\Delta V_1(x=\frac{1}{2})$ for the nonstoichiometric structures are further from experiment. Moreover, while the formation energies $\Delta E_{12}(x=\frac{1}{2})$ are calculated to be positive (unstable) in the experimental geometries, the formation energy of structure *A* is calculated to be negative (stable) in the relaxed geometry. We have not optimized the structure *B* material, but since it has a higher total energy than structure *A* for the experimental structure, we expect it to be less stable. The fact that the calculations find at least one stable nonstoichiometric structure is inconsistent with the experimental findings. The failure of LSDA calculations to correctly model the instability of nonstoichiometric Li_xFePO_4 materials was recently also reported by Zhou and co-workers.[16,49]

C. Results for one-electron spectra

The self-consistent calculations balance the electrostatic and quantum-mechanical interactions within the density-functional model. By analyzing the one-electron spectra in terms of the partial densities of states, one can develop a qualitative picture of the various contributions to the self-consistent results and of the bonding characteristics of these materials. In this section, all calculations were done using the experimental structures.

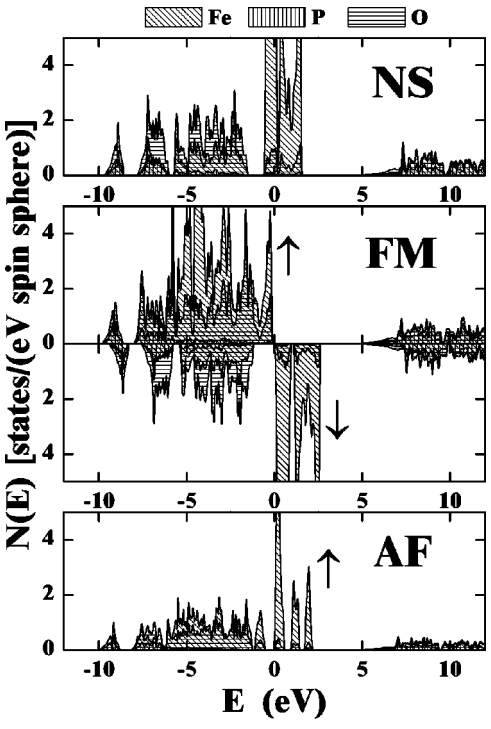

FIG. 2. Partial density of states for $FePO_4$ calculated using the LSDA spin-correlation functional with the indicated spin configurations. The partial densities of states are weighted with the charge within a muffin-tin sphere, averaged over sites of each atomic type. The zero of energy is taken as the Fermi level.

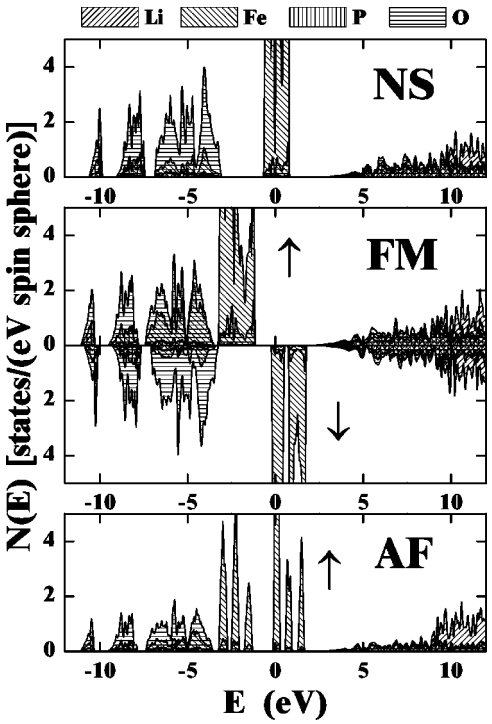

FIG. 3. Partial density of states for $LiFePO_4$ calculated with the indicated spin configurations using same conventions as in Fig. 2.

Figures 2 and 3 show the partial density of states of $FePO_4$ and $LiFePO_4$ for all three spin configurations. In this energy range, the partial density of states associated with the Fe sites are primarily of $3d$ character while the partial density of states associated with the O sites are primarily of $2p$ character.

The NS configuration for both materials shows the Fermi level to lie within the narrow Fe $3d$ band which is well separated from the other states of the system. The fact that this configuration is unable to support appreciable interaction between the Fe $3d$ states and the other states of the system undoubtedly contributes to its instability.

The FM results indicate that $LiFePO_4$ is metallic with the Fermi level falling within the Fe $3d$ bands, while $FePO_4$ has a band gap at the Fermi level. The magnitude of the band gap is less than 0.1 eV for the LSDA calculation, but roughly 0.4 eV for the GGA calculation, as is consistent with the results reported by Yamada.[15] The FM results show the majority spin states associated with the Fe sites ($\uparrow$) separated from the minority spin states ($\downarrow$) at higher energy. For the AF configuration, only the $\uparrow$ contributions are plotted, since the $\downarrow$ distribution is identical. The AF partial density of states shows similar overall band widths and alignments to that of the FM distributions. The states which correspond to majority and minority Fe states in the FM configuration are realized as states localized on the two inequivalent Fe sites in the AF configuration. Since the partial densities of states were weighted with the average charge in each muffin-tin sphere, the peak heights for the AF Fe partial density of states plots appear to be roughly half the corresponding heights for the FM results. Apparently, the crystal-field splittings of the Fe d bands are more pronounced in the AF configuration than in the FM configuration. Since the Fe site is in an approximately octahedral environment due to the neighboring O^{-2} ions, the $3d$ states are split into states of t_{2g} and e_g symmetries. Deviations from octahedral symmetry and molecular interaction with the O $2p$ orbitals cause further splittings.[15]

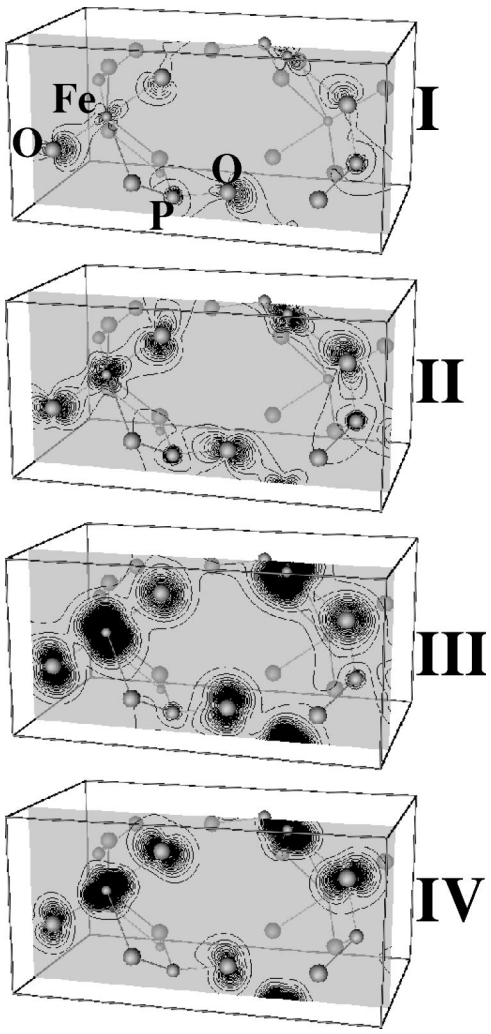

FIG. 4. Electron-density contour plots for majority electrons in $FePO_4$ in four energy ranges. The contours are shown in a plane perpendicular to the **b** axis passing through P—O and Fe—O bonds. Atomic positions are shown with spheres of increasing radius in the order Fe $<$P$<$O. Contour levels are given as multiples of $0.05e/Å^3$. The energy ranges were taken to be I, -9.9 to -8.6; II, -8.1 to -6.2; III, -6.2 to -2.3; and IV, -2.3 to -0.1 eV.

In order to examine the general features of the electronic states of these systems in more detail, it is useful to visualize electron-density contour plots in the distinct regions of the spectrum of occupied states. For this purpose, we focus on the majority electron-spin density in four energy ranges enumerated in Figs. 4 and 5. For both materials energy ranges I and II correspond to states primarily associated with the P—O bonds, showing hybridization with P $3s$ and $3p$ orbitals, respectively. In the energy ranges III and IV are states of primarily O $2p$ and Fe $3d$ character. The interesting difference between the $FePO_4$ and $LiFePO_4$ distributions is the

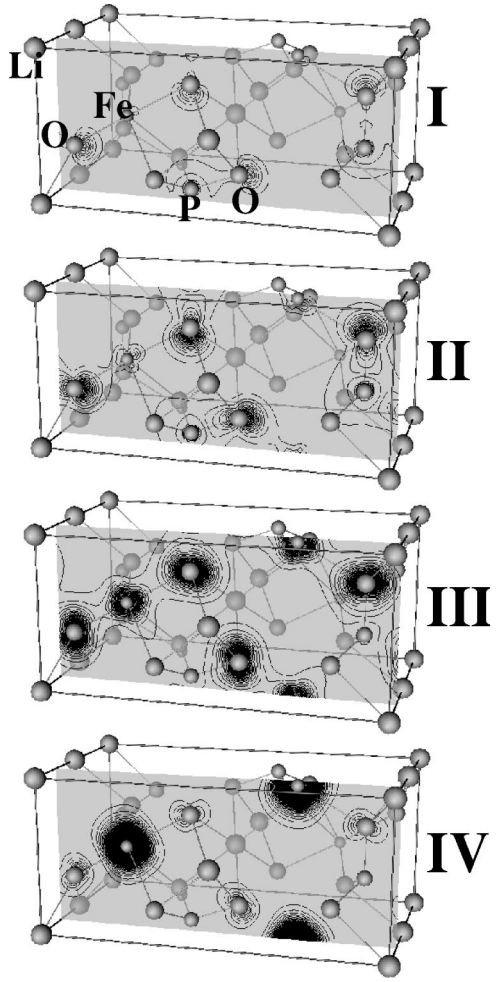

FIG. 5. Electron-density contour plot for majority electrons in $LiFePO_4$ using the same notation and units as in Fig. 4. The energy ranges were taken to be I, -11.2 to -10.2; II, -9.6 to -7.7; III, -7.5 to -3.4; and IV, -3.3 to -1.1 eV.

degree of overlap between the O $2p$ and Fe $3d$ in the majority spin states.

For $FePO_4$, the Fe states are well hybridized with O $2p$ states throughout the valence band. This is seen both in the partial densities of states plots of Fig. 2 and in the contour plots of Fig. 4.

By contrast, for $LiFePO_4$, the partial densities of states of Fig. 3 and the contour plots of Fig. 5 show that the lower valence band (III) is primarily due to the O $2p$ states, while the Fe $3d$ states form a relatively narrow band in range IV. The contour plots of Fig. 5 show a small amount of Fe—O bonding in range III, while in range IV, the contours are mainly about the Fe sites.

The orbital orientations of the densities in regions III and IV of Figs. 4 and 5 are also interesting. The orbitals on the Fe sites are mixtures of t_{2g} and e_g states, which can be seen by plotting the contours for smaller energy ranges. For both materials, the range III states are formed from mostly bonding Fe—O molecular orbitals, while the range IV states are formed from mostly antibonding Fe—O molecular orbitals.

For the FM configuration of both $FePO_4$ and $LiFePO_4$, the density of states plots of Figs. 2 and 3 show that the occupied minority spin states have a smaller contribution from the Fe $3d$ orbitals. In both materials, the minority spin Fe $3d$ states form a narrow band which splits into states of t_{2g} and e_g character, and which is unoccupied in $FePO_4$ and partially occupied in $LiFePO_4$. Above the Fe $3d$ bands, both materials have conduction bands formed from antibonding states of both P—O and Fe—O bonds which have very little spin polarization.

Padhi and co-workers[1,50] pointed out that the Fe—O bond in these materials is affected by the ''inductive effect'' of P. In order to better understand this ''inductive effect'' and the apparently greater covalency of the Fe—O bond in $FePO_4$ relative to the bond in $LiFePO_4$, it is useful to develop a simple model that can analyze the basic interactions between the O $2p$ and Fe $3d$ states. This model focuses on the energy alignment of the O $2p$ states (primarily $\varepsilon_{p\pi}$) with respect to the Fe $3d$ states (ε_d), from which the molecular orbitals are formed. The basic assumption is that the closer these states are energetically, the larger their interaction and covalent bonding. The O $2p$ electrons are most strongly attracted to both the nearest-neighbor P^{+q_P} and $Fe^{+q_{Fe}}$ ions with an electrostatic potential of the form

$$\Delta\mathcal{H} = -\frac{e^2 q_P}{|\mathbf{r}-\mathbf{R}_P|} - \frac{e^2 q_{Fe}}{|\mathbf{r}-\mathbf{R}_{Fe}|}. \tag{9}$$

In this expression, $\mathbf{R}_P$ and $\mathbf{R}_{Fe}$ denote the O—P and O—Fe bond vectors, respectively. These vectors take slightly different values for inequivalent bonds within each material and are slightly different for the two materials, with average values of $R_P \approx 1.5$ Å and $R_{Fe} \approx 2.0$ Å and with an average angle of 130° between the two bonds. The ionic charge for P^{+q_P} is formally $q_P = 5$, although perhaps a smaller charge would fit the model better. The ionic charge for $Fe^{+q_{Fe}}$ is formally $q_{Fe} = 3$ for $FePO_4$ and $q_{Fe} = 2$ for $LiFePO_4$. Apart from the long-range monopole contributions of Eq. (9), the main effect of this interaction is to split the O $2p$ states into three different states. What is significant here is that the Fe potential term is larger for $FePO_4$ than for $LiFePO_4$ resulting in a larger splitting of the O $2p$ states in $FePO_4$ than for $LiFePO_4$. In order to estimate the magnitude of the effect, we can use degenerate perturbation theory to formulate the matrix elements $\langle m|\Delta\mathcal{H}|m'\rangle$, where the azimuthal quantum number for O $2p$ states is given by $m = 0, \pm 1$. The eigenvalues of this matrix approximate the splittings of the O $2p$ states. Since the P^{+q_P} is closer to the O site and has greater charge, the P potential interaction dominates the interaction, but the Fe potential contribution is not negligible. Depending on reasonable parameter choices, we find the splitting of the extreme eigenvalues of Eq. (9) to be between 5 and 8 eV for $FePO_4$ and ≈ 1 eV less for $LiFePO_4$. This means that for $FePO_4$, the electrostatic interactions of the near neighbors cause the O $2p$ band width to be larger than that of $LiFePO_4$. The other ingredient of the model is the energy ε_d of the Fe $3d$ state in these materials, which is most strongly affected by the total charge on the Fe site. Within this simple model that charge is $8-q_{Fe}$. Since this charge screens the electrostatic potential on the Fe site, the orbital energy ε_d decreases with decreasing $8-q_{Fe}$. We expect $\varepsilon_d(FePO_4)$

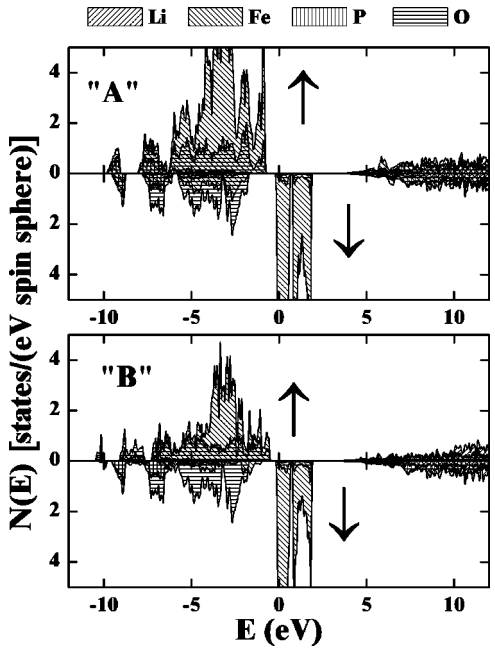

FIG. 6. Partial density of states for ferromagnetic spin configurations and *"A"* and *"B"* geometries of $Li_{1/2}FePO_4$ using same notation as in Fig. 2.

$<\varepsilon_d(\mathrm{LiFePO_4})$ for this reason. Thus, both the increased band width of the O $2p$ band and the lowering of the $3d$ energy level for $FePO_4$ act to increase the energetic overlap of the two states and increase their covalent bonding. This analysis is consistent with the partial density of states results, which show the O $2p$ states to be spread over a larger energy range and more thoroughly mixed with the Fe $3d$ states for $FePO_4$. By contrast, for $LiFePO_4$, the Fe $3d$ states form a separate narrow band of states above the O $2p$ bands.

In Fig. 6 we show the partial densities of states in the ferromagnetic spin configuration for two possible idealized structures of the delithiated material $Li_{1/2}FePO_4$. The results look very similar to each other. In both cases, the majority spin Fe $3d$ states are well mixed with the O $2p$ states, similar to the distribution in $FePO_4$, although the minority Fe $3d$ states are slightly occupied as in the case of $LiFePO_4$.

In Fig. 7 we show the partial densities of states in the ferromagnetic spin configuration for three other members of the LiMPO$_4$ family of materials. The general features of these densities of states and corresponding plot in Fig. 3 are very similar, showing the rigid band filling of the $3d$ bands in accordance with the transition metal series across the periodic table. Interestingly, in all of the fully lithiated materials, the transition metal $3d$ bands form well-defined narrow bands (with bandwidths ≈ 2 eV including crystal-field splittings) unlike the well-mixed Fe $3d$—O$2p$ bands found for the majority spin states of $FePO_4$. The crystal-field splittings of the minority spin $3d$ states appear to be greater for $LiCoPO_4$ and $LiNiPO_4$.

The band structures for the ferromagnetic forms of $FePO_4$ and $LiFePO_4$ are shown in Figs. 8 and 9. The valence bands are very dense with little dispersion. By contrast the conduction bands for both materials have distinctive and almost

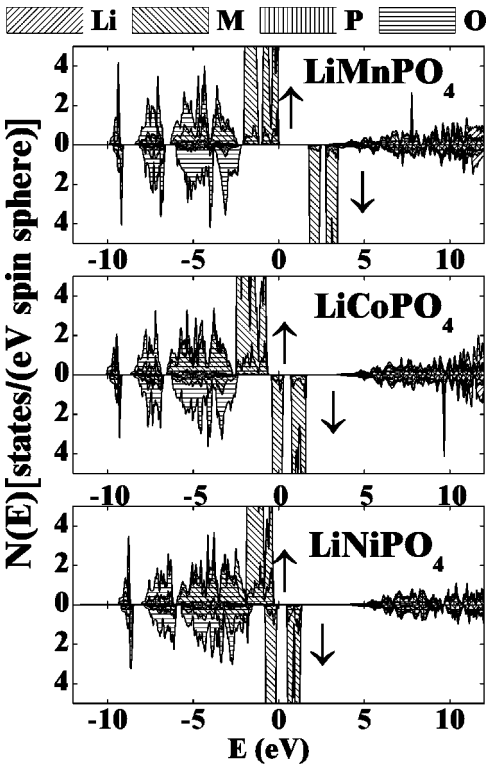

FIG. 7. Partial density of states for ferromagnetic spin configurations of LiMPO$_4$ for $M=$ Mn, Co, and Ni, using same notation as in Fig. 3.

identical dispersions. The minimum in the lowest band occurs at the Γ point. The conduction bands are composed of antibonding states associated with the P—O and Fe—O states which also include Li $2s$ states for $LiFePO_4$. To the extent that these states approximate real quasiparticle states of the system, they could provide states of high electron mobility. Unfortunately, since these states lie considerably above the Fermi level, it would be difficult to access them under low-voltage conditions. Interestingly, the band structures of the other LiMPO$_4$ materials are very similar to those of $LiFePO_4$, with very flat dispersions for the O $2p$ and Fe

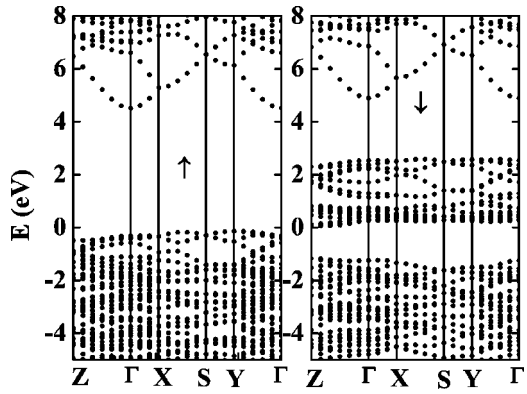

FIG. 8. Electronic band structure of $FePO_4$ in the FM configuration for the majority spin ($\uparrow$) and minority spin ($\downarrow$) states. The labels are those of Koster,[51] with $Z=\pi/c\hat{\mathbf{c}}$, $\Gamma=0$, $X=\pi/a\hat{\mathbf{a}}$, $S=\pi/a\hat{\mathbf{a}}+\pi/b\hat{\mathbf{b}}$, and $Y=\pi/b\hat{\mathbf{b}}$.

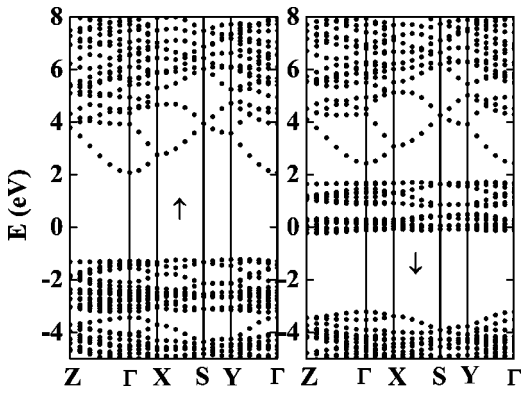

FIG. 9. Electronic band structure of $LiFePO_4$ in the FM configuration using the same notation as in Fig. 8.

$3d$ bands and with the conduction bands having the same distinctive shape as seen in Figs. 8 and 9. Unfortunately, these dispersive conduction bands are well above the Fermi level for all of the materials studied.

V. SUMMARY AND CONCLUSIONS

The results of these calculations have revealed some the important features of the electronic states of $FePO_4$ and $LiMPO_4$. Not surprisingly, spin polarization plays an essential role in stabilizing the electronic states. While these have antiferromagnetic ground states at low temperature, and paramagnetic configurations with measurable magnetic moments associated with the transition metal sites at room temperature, we have argued that reasonable qualitative results can be obtained by studying ferromagnetic models. Partial justification for this is based on the similarities in the densities of states for the ferromagnetic and antiferromagnetic configurations. We have analyzed the partial densities of states which suggest that majority spin states of $FePO_4$ have substantial covalent character due to the energetic overlap of the O $2p$ states with the Fe $3d$ states. In $LiMPO_4$, there is less covalent character such that the M $3d$ states form narrow bands above the O $2p$ bands with relatively little mixing. The results also show that despite its reduced covalency, $LiFePO_4$ is more stable relative to $FePO_4$ and Li metal, and the approximate open circuit voltage for the cathode discharge is calculated to be ≈ 3.2 V, which is comparable to (although smaller than) the experimental value.

The partial density of states and electron contour plots also show that the P—O bonds form states below the main part of the O $2p$ bands. The notion that the strong P—O bonds reduce the covalency of the Fe—O bonds was discussed in an early paper by Padhi and co-workers.[50] The general form of the density of states results are consistent with earlier work of Yamada.[15]

There is a lot of additional work that needs to be done. Recent experimental efforts[6,7,40] have focused on alloying and doping the materials to improve the electrical conductivity especially for the fully charged ($FePO_4$) state and computational modeling could hopefully help this effort. One very basic question that needs to be answered is how the Li^+ ion moves through the crystal, especially, in view of the instability of the Li_xFePO_4. It may be that more sophisticated treatments of the electron correlation effects may be necessary to adequately model the phase diagram of these materials.[16,49]

ACKNOWLEDGMENTS

We would like to thank Dr. Cynthia S. Day for helping us search the crystal databases. The idea for this work was inspired by a talk given by G. Ceder at the ES2002-Fourteenth Annual Workshop on Recent Developments in Electronic Structure Methods, June 6–8th, 2002. We also benefited from helpful discussions with Dr. M. Cococcioni and Professor F. Salsbury. We would also like to thank F. Zhou for sending a copy of his paper, Ref. 49, prior to publication.

*Electronic address: natalie@wfu.edu; www.wfu.edu/~natalie

[1] A.K. Padhi, K.S. Nanjundaswamy, and J.B. Goodenough, J. Electrochem. Soc. **144**, 1188 (1997).
[2] J.M. Tarascon and M. Armond, Nature (London) **414**, 359 (2001).
[3] G.M. Ehrlich, in *Handbook of Batteries*, 3rd ed., edited by D. Linden and T.B. Reddy (McGraw-Hill, New York, 2002), Chap. 35.
[4] *Lithium Ion Batteries; Fundamentals and Performance*, edited by M. Wakihara and O. Yamamoto (Kodansha, Tokyo, 1998).
[5] J.B. Goodenough, A.K. Padhi, K.S. Nanjundaswamy, and C. Masquelier (unpublished).
[6] S.-Y. Chung, J.T. Blocking, and Y.-M. Chiang, Nat. Mater. **1**, 123 (2002).
[7] A. Yamada, M. Hosoya, S.-C. Chung, Y. Kudo, K. Hinokuma, K.-Y. Liu, and Y. Nishi, J. Power Sources **5299**, 1 (2003).
[8] S. Yang, Y. Song, K. Ngala, P.Y. Zavalij, and M.S. Whittingham, J. Power Sources **5300**, 1 (2003).
[9] D. Vaknin, J.L. Zarestky, L.L. Miller, J.-P. Rivera, and H. Schmid, Phys. Rev. B **65**, 224414 (2002).
[10] I. Kornev, M. Bichurin, J.-P. Rivera, S. Gentil, H. Schmid, A.G.M. Jansen, and P. Wyder, Phys. Rev. B **62**, 12 247 (2000).
[11] R.P. Santoro and R.E. Newnham, Acta Crystallogr. **22**, 344 (1967).
[12] M.C. Tucker, M.M. Doeff, T.J. Richardson, R. Fiñones, E.J. Cairns, and J.A. Reimer, J. Am. Chem. Soc. **124**, 3832 (2002).
[13] P. Hohenberg and W. Kohn, Phys. Rev. **136**, B864 (1964).
[14] W. Kohn and L.J. Sham, Phys. Rev. **140**, A1133 (1965).
[15] A. Yamada and S.-C. Chung, J. Electrochem. Soc. **148**, A960 (2001).
[16] F. Zhou, C. Marianetti, M. Cococcioni, D. Morgan, and G. Ceder (unpublished).
[17] P. Tang and N. A. W. Holzwarth (unpublished).
[18] M.K. Aydinol, A.F. Kohan, G. Ceder, K. Cho, and J. Joannopoulos, Phys. Rev. B **56**, 1354 (1997).
[19] C. Wolverton and A. Zunger, Phys. Rev. B **57**, 2242 (1998).
[20] A.V. der Ven, M.K. Aydinol, G. Ceder, G. Kresse, and J. Hafner, Phys. Rev. B **58**, 2975 (1998).
[21] A.V. der Ven, G. Ceder, M. Asta, and T.D. Tepesch, Phys. Rev. B **64**, 184307 (2001).
[22] M.E.A. y de Dompablo, A.V. der Ven, and G. Ceder, Phys. Rev. B **66**, 064112 (2002).

[23] P. Blaha, K. Schwarz, G. Madsen, D. Kvasnicka, and J. Luitz, computer code WIEN2K (Karlheinz Schwarz, Techn. Universität Wien, Austria, 2001); see, http://www.wien2k.at
[24] O.K. Andersen, Phys. Rev. B **12**, 3060 (1975).
[25] G.K.H. Madsen, P. Blaha, K. Schwarz, E. Sjöstedt, and L. Nordström, Phys. Rev. B **64**, 195134 (2001).
[26] P.E. Blöchl, O. Jepsen, and O.K. Andersen, Phys. Rev. B **49**, 16 223 (1994).
[27] J.P. Perdew and Y. Wang, Phys. Rev. B **45**, 13 244 (1992).
[28] J.P. Perdew, K. Burke, and M. Ernzerhof, Phys. Rev. Lett. **77**, 3865 (1996).
[29] R.W. Godby, M. Schlüter, and L.J. Sham, Phys. Rev. B **37**, 10 159 (1988).
[30] J.P. Perdew and A. Zunger, Phys. Rev. B **23**, 5048 (1981).
[31] H.D. Megaw, *Crystal Structures: A Working Approach* (Saunders, London, 1973), Chap. 11.9.
[32] *International Tables for Crystallography, Volume A: Space-Group Symmetry*, edited by T. Hahn, 5th revised ed. (Kluwer, Dordrecht, 2002).
[33] A. Kokalj, J. Mol. Graphics Modell. **17**, 176 (1999).
[34] O. Johnsen, *Minerals of the World* (Princeton University Press, Princeton, NJ, 2002).
[35] F.H. Allen, Acta Crystallogr., Sect. B: Struct. Sci. **B58**, 380 (2002).
[36] R. Mittal, S.L. Chaplot, A.I. Kolesnikov, C.-K. Loong, O.D. Jayakumar, and S.K. Kulshreshtha, Phys. Rev. B **66**, 174304 (2002).
[37] A.S. Andersson, B. Kalska, L. Häggström, and J.O. Thomas, Solid State Ionics **130**, 41 (2000).
[38] O. García-Moreno, M. Alvarez-Vega, F. García-Alvarado, J. García-Jaca, J.M. Gallardo-Amores, M.L. Sanjuán, and U. Amador, Chem. Mater. **13**, 1570 (2001).
[39] N. Ravet, Y. Chouinard, J.F. Magnan, S. Besner, M. Gautheir, and M. Armand, J. Power Sources **97-98**, 503 (2001).
[40] J. Barker, J.Y. Saidi, and J.L. Swoyer, Electrochem. Solid-State Lett. **6**, A53 (2003).
[41] V.A. Streltsov, E.L. Belokoneva, V.G. Tsirelson, and N.K. Hansen, Acta Crystallogr., Sect. B: Struct. Sci. **B49**, 147 (1993).
[42] A.S. Andersson and J.O. Thomas, J. Power Sources **97-98**, 498 (2001).
[43] F. Kubel, Z. Kristallogr. Mineral. **209**, 755 (1994).
[44] R.E. Newnham, R.P. Santoro, and M.J. Redman, J. Phys. Chem. Solids **26**, 445 (1965).
[45] R.P. Santoro, D.J. Segal, and R.E. Newnham, J. Phys. Chem. Solids **27**, 1192 (1966).
[46] J.G. Creer and G.J. Troup, Phys. Lett. **32A**, 439 (1970).
[47] Quoted value is the vector average of the three experimental components.
[48] C. Kittel, *Introduction to Solid State Physics*, 7th ed. (Wiley, New York, 1996), pp. 23–23.
[49] F. Zhou, C.A. Marianetti, M. Cococcioni, D. Morgan, and G. Ceder (private communication).
[50] A.K. Padhi, K.S. Nanjundaswamy, C. Masquelier, S. Okada, and J.B. Goodenough, J. Electrochem. Soc. **144**, 1609 (1997).
[51] G.F. Koster, in *Solid State Physics*, edited by F. Seitz and D. Turnbull (Academic Press, New York, 1957), Vol. 5, pp. 173–256.